

Integrating Inertial Sensors with GPS for Vehicle Dynamics Control

(Journal of Dynamic Systems, Measurement, and Control, June 2004)

Jihan Ryu and J. Christian Gerdes

Department of Mechanical Engineering
Design Division
Stanford University
Stanford, CA 94305-4021, USA
E-mail: {jihan, gerdes}@stanford.edu

ABSTRACT

This paper demonstrates a method of estimating several key vehicle states – sideslip angle, longitudinal velocity, roll and grade – by combining automotive grade inertial sensors with a Global Positioning System (GPS) receiver. Kinematic Kalman filters that are independent of uncertain vehicle parameters integrate the inertial sensors with GPS to provide high update estimates of the vehicle states and the sensor biases. Using a two-antenna GPS system, the effects of pitch and roll on the measurements can be quantified and are demonstrated to be quite significant in sideslip angle estimation. Employing the same GPS system as an input to the estimator, this paper develops a method that compensates for roll and pitch effects to improve the accuracy of the vehicle state and sensor bias estimates. In addition, calibration procedures for the sensitivity and cross-coupling of inertial sensors are provided to further reduce measurement error. The resulting state estimates compare well to the results from calibrated models and Kalman filter predictions and are clean enough to use in vehicle dynamics control systems without additional filtering.

1. INTRODUCTION

While new steering and braking actuator designs provide new opportunities to shape vehicle dynamics through active control, the primary challenge in the development of vehicle control systems remains the lack of necessary feedback. In particular, the difficult problem of estimating the sideslip angle or lateral velocity of the vehicle currently limits the algorithms that can be incorporated in production systems. Although vehicle stability and steering control systems require sideslip angle for their control purposes [1-3] and future steer-by-wire systems will require it for full-state feedback [4], current vehicles are not equipped with an ability to measure the sideslip angle directly. As a result, the sideslip angle must instead be estimated for vehicle control applications. Two common techniques for estimating the sideslip angle are integrating an automotive grade accelerometer and rate gyro directly and using a physical vehicle model as an observer [3,5]. Some methods use a combination or switch between these two methods appropriately based on vehicle states [1,3]. While they have enabled vehicle dynamics control in series production, these solutions nevertheless have fundamental problems. Direct integration methods can

accumulate sensor errors and unwanted measurements from road grade and bank angle (superelevation) while methods based on a physical vehicle model can be sensitive to changes in the vehicle parameters and inaccurate on low friction surfaces [6]. The vehicle control systems of the future, therefore, will only be enabled by improvements in sensing.

Since the vehicle sideslip angle is the difference between the vehicle yaw angle and the direction of the velocity, the sideslip angle can be calculated if both the attitude and velocity of the vehicle are known. Inertial Navigation Systems (INS), commonly used in aviation applications, could provide these values by integrating gyro measurements to get the attitude and integrating accelerometer measurements with gravity compensation to get the velocity [7-9]. In general, integration of inertial measurements is limited only by the drift in sensor bias and sensitivity, and sensor quality or grade is judged according to this drift rate. To estimate the vehicle yaw angle over long periods of time with enough accuracy for sideslip angle determination using INS alone would require a tactical or navigation grade system with a drift rate from 1 deg/hr to 0.01 deg/hr. With a cost of \$10,000 or more [10], such a system is much too expensive for automotive applications. However, integration with velocity measurements from the Global Positioning System (GPS) can effectively negate these drift effects and enable the use of lower grade INS sensors.

GPS velocity is considerably more accurate than position, with errors on the order of 3 cm/s (1σ , horizontal) and 6 cm/s (vertical) even without differential corrections [11]. The integration of INS sensors with GPS has been given much attention, especially in aircraft applications, due to the complementary nature of the individual systems. GPS measurements are stable but subject to a fairly low update rate and signal blockage while inertial sensor measurements are continuously available but suffer from long term drift. In aircraft, this combination has been used to update position, velocity, and attitude estimates with inertial equipment between GPS measurements [7,8] and to dead reckon with inertial sensors alone during GPS outages [9,12]. Spurred by the increase in GPS systems in cars, Bevely and colleagues developed a method of estimating vehicle sideslip by integrating inertial sensors from a stability control system with a single antenna GPS using a planar vehicle model [11,13]. With the planar model, out-of-plane vehicle motions due to roll and pitch could not be taken into account, leaving open questions of system accuracy and the potential benefits of additional sensing.

This paper investigates the use of several sensor configurations and levels of modeling fidelity in the estimation of vehicle sideslip. Unlike previous work, the vehicle yaw information is obtained from a two-antenna GPS system that not only eliminates issues of drift in attitude estimation but also provides a measurement of the roll angle. Using this system, the paper investigates the influence of road grade, bank angle, and vehicle roll on GPS-based vehicle sideslip and longitudinal velocity estimates derived from a planar model. Since roll and grade have a pronounced effect [14], this paper proposes a new method of estimating several key vehicle states (sideslip angle, longitudinal velocity, yaw, and roll) using the two-antenna GPS system in combination with inertial sensors. The combined system fuses a road grade estimate derived from GPS velocity [15] and the roll information from the two-antenna system with an appropriate roll center model of the vehicle.

Comparisons with a calibrated vehicle model show excellent correlation and the relative constancy of the sensor bias estimates demonstrates that no significant dynamics are ignored. From a practical standpoint, this paper also describes a couple of refinements to calibrate sensitivity variation and cross-coupling of inertial sensors. Statistical analysis demonstrates that the performance of the final system with calibration performs according to the predictions of propagated Kalman filter covariances. The resulting system provides sideslip angle feedback at a level previously unavailable and has been successfully integrated as a state feedback measurement for a steer-by-wire system [4]. With multiple antenna GPS systems currently deployed for automated farming [16] and marine navigation and under development at automotive price points, a sensing system such as this could be the key enabling technology for future vehicle dynamics control systems.

2. PLANAR BICYCLE MODEL AND SIDESLIP

While the Kalman filters to be developed rely only on the kinematics of vehicle motion, a dynamic model is required for validating the filter performance. The lateral dynamics of a vehicle in the horizontal plane are represented here by the single track, or bicycle model with states of lateral velocity, u_y , and yaw rate, r . The bicycle model is a standard representation in the area of ground vehicle dynamics and has been used extensively in previous work [1,4-6,13,14]. While detailed derivation and explanation can be found in many textbooks [17,18], the underlying assumptions are that the slip angles on the inside and outside wheels are approximately the same and the effect of the vehicle roll is small. These assumptions hold well for most typical (non-emergency) driving situations and, in particular, for the test maneuvers used for validation in this paper.

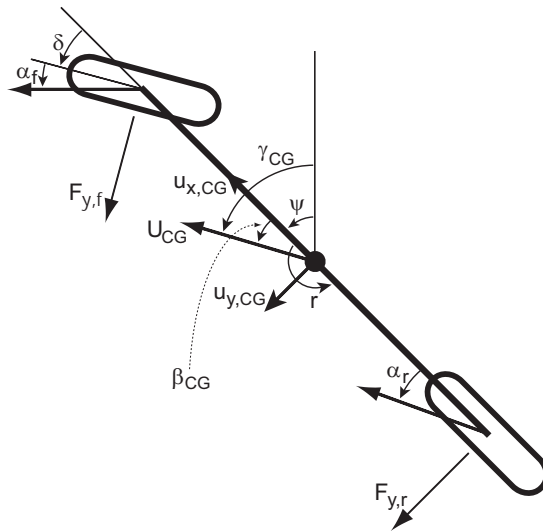


Figure 1 Bicycle Model

In Fig. 1, δ is the steering angle, u_x and u_y are the longitudinal and lateral components of the vehicle velocity, F_{yf} and F_{yr} are the lateral tire forces, and α_f and α_r are the tire slip angles. The state equation for the bicycle model can be written as:

$$\begin{bmatrix} \ddot{u}_{y,CG} \\ \dot{r} \end{bmatrix} = \begin{bmatrix} \frac{-C_{af}-C_{ar}}{mu_{x,CG}} & -u_{x,CG} + \left(\frac{C_{ar}b-C_{af}a}{mu_{x,CG}}\right) \\ \frac{C_{ar}b-C_{af}a}{I_z u_{x,CG}} & \frac{-C_{af}a^2-C_{ar}b^2}{I_z u_{x,CG}} \end{bmatrix} \begin{bmatrix} u_{y,CG} \\ r \end{bmatrix} + \begin{bmatrix} \frac{C_{af}}{m} \\ \frac{C_{af}a}{I_z} \end{bmatrix} \delta \quad (1)$$

I_z is the moment of inertia of the vehicle about its yaw axis, m is the vehicle mass, a and b are distance of the front and rear axles from the CG, and C_{af} and C_{ar} are the total front and rear cornering stiffness. The assumption that both the slip angle and the cornering stiffness are approximately the same for the inner and outer tires on each axle is inherent in this model.

Given the longitudinal and lateral velocities, u_x and u_y , at any point on the vehicle body, the sideslip angle can be defined by:

$$\beta = \tan^{-1}\left(\frac{u_y}{u_x}\right) \quad (2)$$

The sideslip angle at the center of gravity (CG) is shown by β_{CG} in Fig. 1. The sideslip angle can also be defined as the difference between the vehicle yaw angle (ψ) and the direction of the velocity (γ) at any point on the body.

$$\beta = \gamma - \psi \quad (3)$$

Since a two-antenna GPS receiver provides both velocity and attitude measurements, the vehicle yaw angle and direction of the velocity can be directly measured. In the flat world of the bicycle model, therefore, the sideslip angle can be calculated by simply using Eq. (3). The errors introduced by this simplification are discussed in subsequent sections.

3. GPS/INS INTEGRATION USING KALMAN FILTERS

3.1 General Kalman Filter Structure

Because the update rate of most GPS receivers is not high enough for control purposes [13], INS sensors are commonly integrated with GPS measurements in a Kalman filter structure to provide higher update rate estimates of the vehicle states. While the filter could be based around the physical model in Eq. (1), there are some drawbacks to such an approach. Since this model is valid only in the linear region and the parameters involve significant uncertainty, particularly with respect to tire stiffnesses, a Kalman filter built on this model may possess significant estimation error. With the two antenna GPS system, however, it is possible to use two kinematic models, independent of any physical parameter uncertainties and changes, in the state estimator.

The traditional Kalman filter is comprised of a measurement update and a time update. Because of the lower update rate of the GPS measurement, the measurement update is performed only when GPS is available in order to estimate the sensor bias and zero out the state estimation error. The measurement update is generally described by:

$$\begin{aligned} x_+(t) &= x_-(t) + K[y(t) - Cx_-(t)] \\ K &= P_-(t)C^T [CP_-(t)C^T + R]^{-1} \quad \text{or} \quad K = P_+(t)C^T R^{-1} \\ P_+(t) &= [I - KC]P_-(t) \quad \text{or} \quad P_+(t)^{-1} = P_-(t)^{-1} + C^T R^{-1} C \end{aligned} \quad (4)$$

where:

$x_-(t)$ = prior estimate of the system state at time t
 $x_+(t)$ = updated estimate of the system state at time t
 $P_-(t)$ = prior error covariance matrix at time t
 $P_+(t)$ = updated error covariance matrix at time t
 K = Kalman Gain
 $y(t)$ = new measurement
 C = observation matrix
 R = measurement noise covariance

Here x and y represent vehicle states of interest and available measurements, respectively, for a general filter. Simple integration of the inertial sensors is performed during the time update because GPS measurements are not available. Using the discrete model of a sampled-data system, the time update can be written as:

$$\begin{aligned}
 x_-(t+1) &= A_d x_+(t) + B_d u(t) \\
 P_-(t+1) &= A_d P_+(t) A_d^T + Q
 \end{aligned} \tag{5}$$

where:

$$\begin{aligned}
 A_d &= e^{A\Delta T} = \sum_{k=0}^{\infty} \frac{A^k \Delta T^k}{k!} \\
 B_d &= \int_0^{\Delta T} e^{A\eta} d\eta B = \sum_{k=0}^{\infty} \frac{A^k \Delta T^{k+1}}{(k+1)!} B \\
 u(t) &= \text{input to the system at time } t \\
 Q &= \text{process noise covariance}
 \end{aligned}$$

This Kalman filter structure is used for all of the individual filters in the paper.

3.2 State Estimation with Planar Vehicle Dynamics

In previous work with GPS for sideslip estimation [13], the vehicle yaw angle was estimated by integrating a yaw gyro. This is not an ideal approach, however, since the estimate must be periodically reset while driving straight in order to prevent integration of gyro bias error from producing large, fictitious sideslip values. The addition of a two-antenna GPS receiver solves this problem by providing an absolute attitude reference and the opportunity to neatly decouple the estimation problem into two simple Kalman filters. One is used to estimate the vehicle yaw angle without errors arising from gyro integration while the other is used to estimate absolute longitudinal and lateral velocities of the vehicle without using wheel speed sensors.

For the yaw Kalman filter, the kinematic relationship between the yaw rate measurements and the yaw angle can be written as:

$$r_m = \dot{\psi} + r_{bias} + noise \tag{6}$$

where:

$$\begin{aligned}
 \psi &= \text{yaw angle (vehicle heading)} \\
 r_m, r_{bias} &= \text{yaw rate gyro measurement and bias}
 \end{aligned}$$

The yaw angle can be measured using a two-antenna GPS receiver.

$$\psi_m^{GPS} = \psi + noise \tag{7}$$

where:

$$\psi_m^{GPS} = \text{yaw angle measurement from GPS}$$

A linear dynamic system can be constructed from Eq. (6) and Eq. (7) using the inertial sensor as the input and GPS as the measurement.

$$\begin{bmatrix} \dot{\psi} \\ \dot{r}_{bias} \end{bmatrix} = \begin{bmatrix} 0 & -1 \\ 0 & 0 \end{bmatrix} \begin{bmatrix} \psi \\ r_{bias} \end{bmatrix} + \begin{bmatrix} 1 \\ 0 \end{bmatrix} r_m + noise \quad (8)$$

When GPS attitude measurements are available,

$$\psi_m^{GPS} = [1 \quad 0] \begin{bmatrix} \psi \\ r_{bias} \end{bmatrix} + noise \quad (9)$$

The Kalman filter in Eq. (4) and Eq. (5) is then applied to the system to obtain the vehicle yaw angle and the gyro bias. Using Eq. (5), a discrete representation of sampled Eq. (8) can be written exactly as:

$$\begin{aligned} x(t+1) &= A_d x(t) + B_d u(t) \\ A_d &= e^{A\Delta T} = \sum_{k=0}^{\infty} \frac{A^k \Delta T^k}{k!} = \begin{bmatrix} 1 & -\Delta T \\ 0 & 1 \end{bmatrix} \\ B_d &= \int_0^{\Delta T} e^{A\eta} d\eta B = \sum_{k=0}^{\infty} \frac{A^k \Delta T^{k+1}}{(k+1)!} B = \begin{bmatrix} \Delta T \\ 0 \end{bmatrix} \end{aligned} \quad (10)$$

The state vector, x , in this Kalman filter is $[\psi \ r_{bias}]^T$, the input, u , is the measured yaw rate r_m from the yaw rate gyro. The measurement y in the Kalman filter is the yaw angle from GPS, ψ_m^{GPS} , with observation matrix C , which is $[1 \ 0]$ only when GPS measurements are available. The observation matrix C is $[0 \ 0]$ when GPS measurements are not available since the system simply integrates the gyro in this case.

For the velocity Kalman filter, the kinematic relationship between acceleration measurements and velocity components at the point where the sensor is located can be written as:

$$\begin{aligned} a_{x,m} &= \dot{u}_{x,sensor} - \dot{\psi} \cdot u_{y,sensor} + a_{x,bias} + noise \\ a_{y,m} &= \dot{u}_{y,sensor} + \dot{\psi} \cdot u_{x,sensor} + a_{y,bias} + noise \end{aligned} \quad (11)$$

where:

- $u_{x,sensor}$ = longitudinal velocity at sensor location
- $a_{x,m}, a_{x,bias}$ = longitudinal accelerometer measurement and bias
- $u_{y,sensor}$ = lateral velocity at sensor location
- $a_{y,m}, a_{y,bias}$ = lateral accelerometer measurement and bias

The longitudinal and lateral velocity can be estimated using GPS velocity together with the yaw Kalman filter. First, the sideslip angle (β^{GPS}) needs to be calculated using the velocity vector (U^{GPS}) from the GPS measurement and the vehicle yaw angle (ψ) from the yaw Kalman filter by Eq. (3). Then, the longitudinal velocity measurement ($u_{x,m}^{GPS}$) and lateral velocity measurement ($u_{y,m}^{GPS}$) are simply:

$$\begin{aligned} u_{x,m}^{GPS} &= \|U^{GPS}\| \cdot \cos(\beta^{GPS}) \\ u_{y,m}^{GPS} &= \|U^{GPS}\| \cdot \sin(\beta^{GPS}) \end{aligned} \quad (12)$$

Assuming that the primary GPS antenna giving velocity measurements is placed directly above the sensor location, the measured velocity components from GPS can be written as:

$$\begin{aligned} u_{x,m}^{GPS} &= u_{x,sensor} + noise \\ u_{y,m}^{GPS} &= u_{y,sensor} + noise \end{aligned} \quad (13)$$

where:

$$\begin{aligned} u_{x,m}^{GPS} &= \text{longitudinal velocity measurement from GPS} \\ u_{y,m}^{GPS} &= \text{lateral velocity measurement from GPS} \end{aligned}$$

Note that Eq. (13) holds only when the primary GPS antenna is located above the sensor location. If it is not, an additional velocity term from the yaw rate must be taken into account.

A Kalman filter is then applied to the following linear dynamic system from Eq. (11) and Eq. (13) to obtain the vehicle velocities and the sensor biases.

$$\begin{bmatrix} \dot{u}_{x,sensor} \\ \dot{a}_{x,bias} \\ \dot{u}_{y,sensor} \\ \dot{a}_{y,bias} \end{bmatrix} = \begin{bmatrix} 0 & -1 & r & 0 \\ 0 & 0 & 0 & 0 \\ -r & 0 & 0 & -1 \\ 0 & 0 & 0 & 0 \end{bmatrix} \begin{bmatrix} u_{x,sensor} \\ a_{x,bias} \\ u_{y,sensor} \\ a_{y,bias} \end{bmatrix} + \begin{bmatrix} 1 & 0 \\ 0 & 0 \\ 0 & 1 \\ 0 & 0 \end{bmatrix} \begin{bmatrix} a_{x,m} \\ a_{y,m} \end{bmatrix} + noise \quad (14)$$

where:

$$r = \dot{\psi} = r_m - r_{bias} = \text{compensated yaw rate}$$

When GPS velocity measurements are available,

$$\begin{bmatrix} u_{x,m}^{GPS} \\ u_{y,m}^{GPS} \end{bmatrix} = \begin{bmatrix} 1 & 0 & 0 & 0 \\ 0 & 0 & 1 & 0 \end{bmatrix} \begin{bmatrix} u_{x,sensor} \\ a_{x,bias} \\ u_{y,sensor} \\ a_{y,bias} \end{bmatrix} + noise \quad (15)$$

In the Kalman filter of Eq. (4) and Eq. (5), the state vector, x , is $[u_{x,sensor} \ a_{x,bias} \ u_{y,sensor} \ a_{y,bias}]^T$ and the measurement, y , is $[u_{x,m}^{GPS} \ u_{y,m}^{GPS}]^T$. The discrete state space form of Eq. (14) can be represented exactly as:

$$\begin{aligned} A_d = e^{A\Delta T} &= \sum_{k=0}^{\infty} \frac{A^k \Delta T^k}{k!} = \begin{bmatrix} \cos(r \cdot \Delta T) & \frac{-\sin(r \cdot \Delta T)}{r} & \sin(r \cdot \Delta T) & \frac{\cos(r \cdot \Delta T) - 1}{r} \\ 0 & 1 & 0 & 0 \\ -\sin(r \cdot \Delta T) & \frac{1 - \cos(r \cdot \Delta T)}{r} & \cos(r \cdot \Delta T) & \frac{\sin(r \cdot \Delta T)}{r} \\ 0 & 0 & 0 & 1 \end{bmatrix} \\ B_d &= \int_0^{\Delta T} e^{A\eta} d\eta B = \sum_{k=0}^{\infty} \frac{A^k \Delta T^{k+1}}{(k+1)!} B = \begin{bmatrix} \frac{\sin(r \cdot \Delta T)}{r} & \frac{1 - \cos(r \cdot \Delta T)}{r} \\ 0 & 0 \\ \frac{\cos(r \cdot \Delta T) - 1}{r} & \frac{\sin(r \cdot \Delta T)}{r} \\ 0 & 0 \end{bmatrix} \end{aligned} \quad (16)$$

4. EXPERIMENTAL RESULTS - PLANAR MODEL

While the estimator in the previous section is quite simple, it relies heavily on the assumption that motion occurs only in the plane. To determine the validity of this

assumption, a series of experiments was performed on a Mercedes E-class wagon. This test vehicle is equipped with a 3-axis automotive-grade accelerometer/rate gyro triad sampled at 100 Hz. Sensor noise levels (1σ) are 0.05 m/s^2 for the accelerometers and 0.2 deg/s for the rate gyros. The vehicle is also equipped with Novatel GPS antenna/receiver pairs, providing 10 Hz velocity measurements and 5 Hz attitude measurements with a noise level (1σ) of less than 3 cm/s and 0.2 deg respectively.

Because the GPS receiver introduces a half sample period inherent latency and a finite amount of time is needed for computation and data transfer, the time tags in the GPS measurement messages and the synchronizing pulse from the receiver are used to align the GPS information with the inertial sensor measurements. This synchronizing process is very important when the inertial sensors are combined with the GPS measurements, because any time offset between two measurements may result in significant overall estimation errors [13].

Figure 2 shows yaw angle estimates compared to raw GPS measurements. Experimental tests consisting of several laps around an uneven parking lot are performed. Note that integration of inertial sensors fills in the gaps between GPS measurements. Even though the update rate of the GPS measurements is not high enough for vehicle control purposes, the combination of GPS measurements with inertial measurements provides estimates with sufficient bandwidth for vehicle control applications [13].

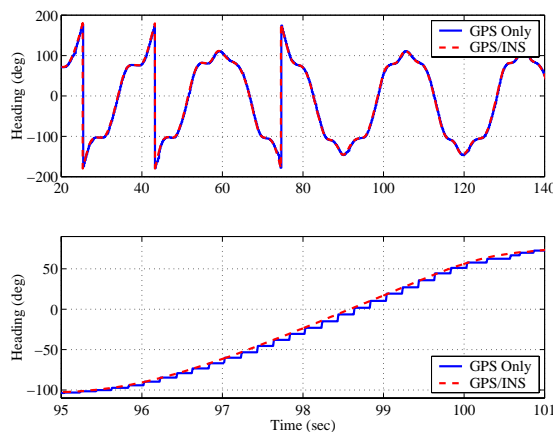


Figure 2 Yaw Angle Estimates

Figure 3 compares yaw rate and sideslip angle estimates from the GPS/INS integration with the results from a carefully calibrated bicycle model. Since the velocity Kalman filter provides the velocity at the sensor location, the velocity estimates are translated to the center of gravity with the yaw rate for comparison with the bicycle model. The similarity between the estimated and model yaw rates demonstrates that the bicycle model used in the comparison is indeed calibrated for the vehicle.

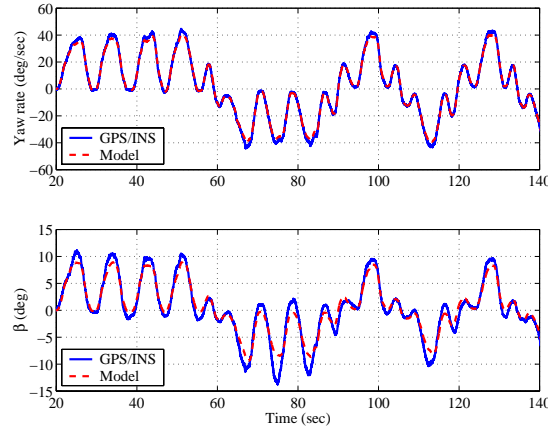


Figure 3 Yaw Rate and Sideslip Angle Estimates

In contrast, there are differences between estimated and modeled sideslip angles. Even though the estimated sideslip is still much better than that obtained from simply integrating the accelerometer [13] – the slip angle estimate is quite clean and does not drift – the accuracy is less than would be desired for control purposes. Not surprisingly, these differences are consistent with the uneven grade and bank angle of the test path – factors neglected in the assumption of planar motion. The correlation between these differences and unevenness of the surface can be seen easily by comparing the accelerometer biases with the surface grade and vehicle roll.

Although some caveats are noted later in the paper, the surface grade can in general be estimated by examining the ratio of the vertical velocity obtained from GPS to the horizontal GPS velocity [15].

$$\theta_r \approx \tan^{-1}\left(\frac{U_V}{U_H}\right) \quad (17)$$

where:

θ_r = road grade estimate

U_V, U_H = vertical and horizontal velocity from GPS

Figure 4 shows the strong correlation between the longitudinal accelerometer bias and the grade along the test path calculated according to the velocity ratio.

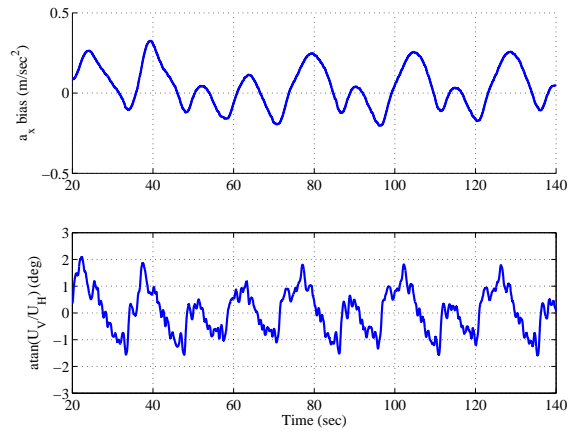


Figure 4 Longitudinal Accelerometer Bias and Grade Estimates

As would be expected, the longitudinal accelerometer bias term reflects the component of gravitational acceleration entering as a result of the grade.

Since the two antennas of the GPS receiver are placed laterally, the combination of road bank angle (sometimes called side-slope or superelevation) and vehicle roll can be directly measured. As shown in Fig. 5, the lateral accelerometer bias and the roll angle show the same correlation as the longitudinal values. The rationale is exactly the same since roll causes a component of the gravitational acceleration to enter the lateral acceleration measurement.

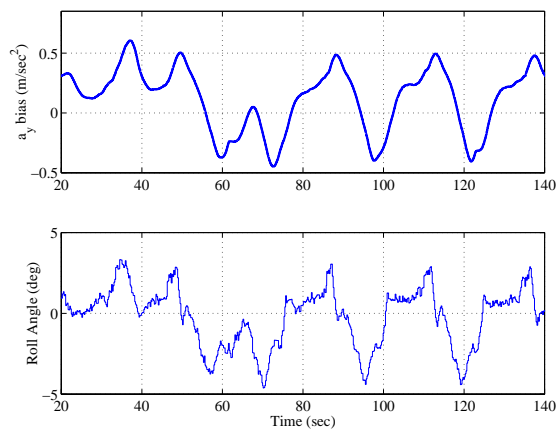


Figure 5 Lateral Accelerometer Bias and Roll Angle

5. ROLL CENTER MODEL WITH ROAD GRADE

For a more accurate estimate of the slip angle it is necessary to compensate for the effects of vehicle pitch and roll. While this could be accomplished in a number of ways – such as incorporating a 3 or 4 antenna GPS system for 3D attitude measurement – basic estimates of roll and grade are available with the existing sensor suite. Assuming that vehicle pitch is caused mostly by road grade, and that grade can be estimated by examining

the velocity ratio using Eq. (17), gravity components in acceleration measurements due to pitch and roll can be compensated using only a two-antenna GPS receiver. Thus the measurements used to demonstrate the correlation between sensor biases and road geometry in the previous section can be harnessed to remove these effects.

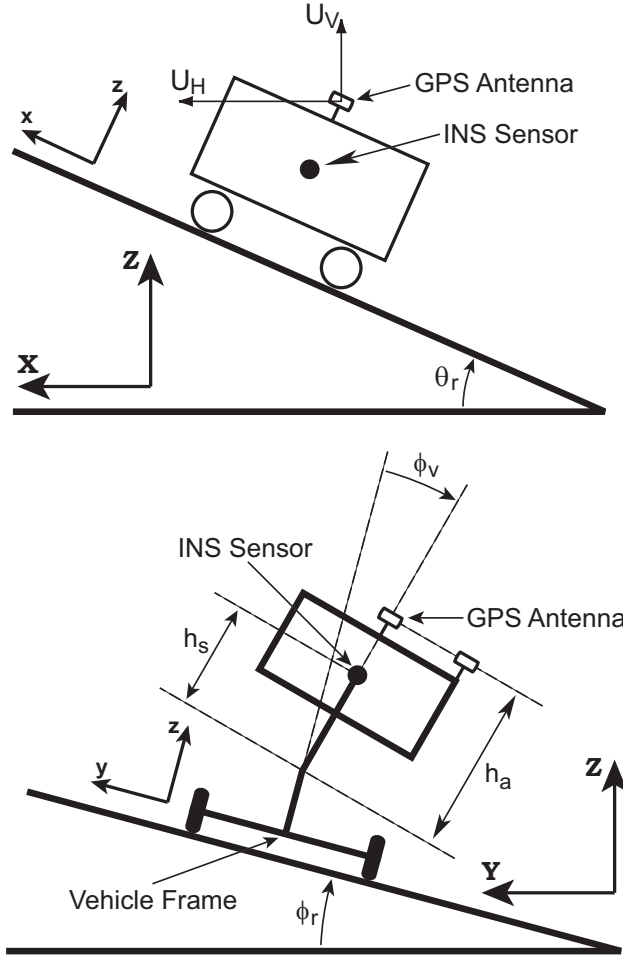


Figure 6 Roll Center Model with Grade and Bank Angle

A roll center vehicle model with a road grade and a bank angle is shown in Fig. 6. This model assumes that the vehicle body rotates about a fixed point (the roll center) on a frame that remains in the plane of the road. The expected gravity component in the acceleration measurement can be explicitly specified and compensated in Eq. (11) because the grade of the surface can be estimated from the GPS velocity measurement and the total roll angle (the sum of the vehicle roll angle and the bank angle or superelevation of the surface) can be measured utilizing the two-antenna GPS receiver.

The kinematic relationship between acceleration measurements and velocity components at the sensor location for this model can be written as:

$$\begin{aligned} a_{x,m} &= \dot{u}_{x,sensor} - \dot{\psi} \cdot u_{y,sensor} + a_{x,bias} + g \cdot \sin \theta_r + noise \\ a_{y,m} &= \dot{u}_{y,sensor} + \dot{\psi} \cdot u_{x,sensor} + a_{y,bias} + g \cdot \sin \phi_t + noise \end{aligned} \quad (18)$$

where:

θ_r = road grade estimate
 $\phi_t = \phi_r + \phi_v$ = sum of road superelevation and vehicle roll

These additional terms can easily be included in the Kalman filter based on Eq. (14) - Eq. (16).

Another important advantage in using the roll center model is that the roll motion of vehicle can be taken into account when determining vehicle velocity. Note that Eq.(18) is written for the point at which the sensor is located and the two GPS antennas are placed on the top of the vehicle roof. Therefore, there is an additional velocity component due to vehicle yaw and roll in the GPS velocity measurement. This can be included by translating the velocity at the antenna to the point at which the sensor is located using Eq. (19) under the assumption of small road grades and bank angles.

$$\begin{aligned} u_{x,m}^{GPS} &= u_{x,sensor} + r \cdot \sin \phi_v \cdot (h_a - h_s) + noise \\ &\approx u_{x,sensor} + noise \\ u_{y,m}^{GPS} &= u_{y,sensor} - p \cdot \cos \phi_v \cdot (h_a - h_s) + noise \\ &\approx u_{y,sensor} - p \cdot (h_a - h_s) + noise \end{aligned} \quad (19)$$

where:

r = yaw rate
 p = roll rate
 h_a = distance from roll center to GPS antenna
 h_s = distance from roll center to INS sensor

Since the vehicle roll angle is small, the additional velocity component is negligible relative to the vehicle longitudinal velocity. However, the additional velocity component due to the roll rate should be considered in the lateral direction since the lateral velocity is comparably small. This roll rate compensation plays an important role when the vehicle is experiencing a heavy roll motion. If the primary GPS antenna is not placed directly above the inertial sensor, the yaw rate of the vehicle should also be taken into account in the lateral velocity measurement.

In addition, the sum of the road bank angle and the vehicle roll can be estimated by constructing a roll Kalman filter in the same manner as in the yaw Kalman filter. Since the GPS antennas and roll gyro are attached to the vehicle body, only the sum of the road bank angle and the vehicle roll angle can be measured without additional modeling. For the roll Kalman filter, the kinematic relationship between roll rate measurements and roll angle can be written as:

$$p_m = \dot{\phi}_t + p_{bias} + noise \quad (20)$$

where:

p_m, p_{bias} = roll rate gyro measurement and bias

The roll angle can be measured using a two-antenna GPS receiver:

$$\phi_m^{GPS} = \phi_t + noise \quad (21)$$

where:

ϕ_m^{GPS} = roll angle measurement from GPS

The roll Kalman filter is then implemented using Eq. (20) and Eq. (21) in the same manner as in the yaw Kalman filter. The state vector, x , is $[\phi_t \ p_{bias}]^T$ and the measurement, y , is the roll angle from GPS, ϕ_m^{GPS} .

6. EXPERIMENTAL RESULTS - ROLL MODEL

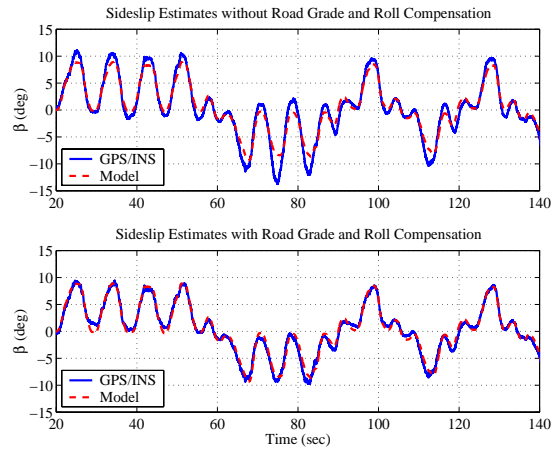


Figure 7 Comparison of Sideslip Angle Estimates

Figure 7 shows the experimental results of sideslip angle estimation with and without the compensation. Since the velocity Kalman filter provides the velocity at the sensor location, whereas the bicycle model generates the sideslip angle at the center of gravity, the velocity estimates from the filter are translated with yaw and roll rates to the corresponding point on the vehicle frame for the comparison with the bicycle model. Note that the discrepancies between the model and estimate are significantly reduced after the compensation. The same improvement can be seen in the case of longitudinal velocity estimation shown in Fig. 8. Differences between the longitudinal velocity estimate and wheel speed after the compensation are, in fact, due to longitudinal slip of the tire.

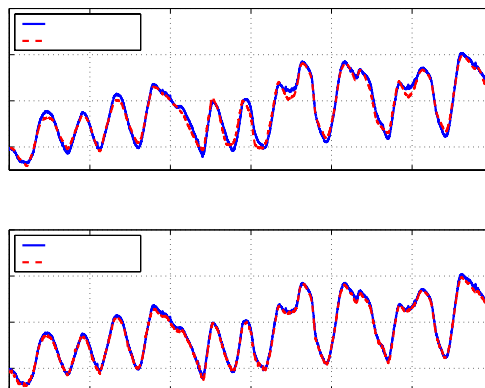


Figure 8 Longitudinal Velocity Estimates

The combination of road bank angle and vehicle roll angle is also estimated using the roll Kalman filter. Figure 9 shows roll estimates together with raw GPS roll measurements. Integration of INS sensors fills in the gaps between GPS measurements giving a smooth roll signal.

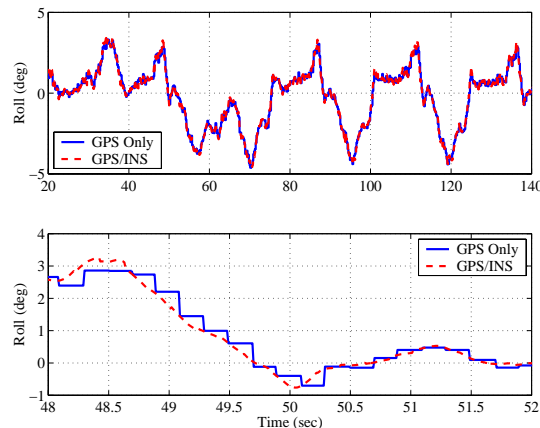


Figure 9 Roll Angle Estimates

With accurate measurements of roll angle and roll rate, it is possible to estimate parameters related to the roll dynamics such as roll stiffness and damping ratio [19]. A dynamic roll model can be used for a wide variety of applications including rollover warning [20] or active suspension control. In addition, a parameterized vehicle roll dynamic model could conceivably be used to separate roll and bank angle.

7. FURTHER REFINEMENTS

7.1 Gyro Sensitivity Effects and Estimation

After the compensation for grade and roll described in the previous sections, both sideslip angle and yaw rate estimates match the model predicted values very well, suggesting that the proposed scheme can correct for changes in grade and roll. However, the estimated sensor biases show significant variations over a short period of time, which is not consistent with the bias estimates representing true electrical biases. These variations can be seen in the following typical experimental results. As Fig. 10 illustrates, considerable low frequency variation exists in the estimated accelerometer bias after compensating for road grade and roll.

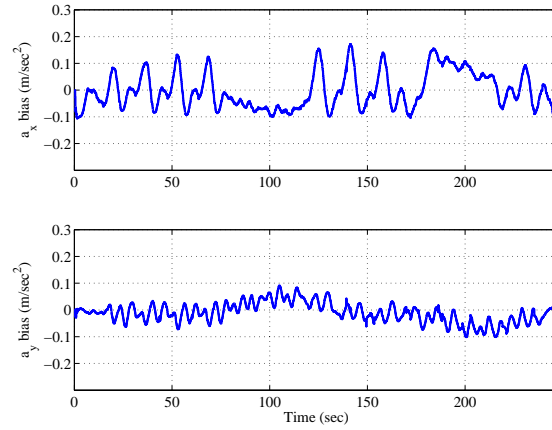


Figure 10 Estimated Accelerometer Biases

These variations in the estimated accelerometer bias can be also seen in the estimated yaw gyro bias in Fig. 11.

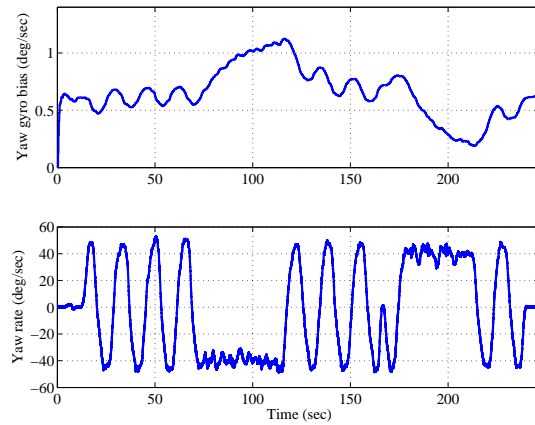


Figure 11 Estimated Yaw Gyro Bias and Yaw Rate

While the bias variation is significant, it is interesting to note that the bias is strongly correlated with the yaw rate. In other words, the yaw gyro bias increases or decreases depending on the sign of the yaw rate. The yaw gyro bias increases when the yaw rate is negative and decreases when the yaw rate is positive. This can easily be seen in Fig. 11 at around 100 and 200 seconds.

The dependency of the bias on the sign of the yaw rate implies that there is an error in the sensitivity (scale factor) of the yaw rate gyro. In order to resolve this problem, a new sensor kinematic relationship that includes both sensitivity and bias is used:

$$r_m = s_r \cdot \dot{\psi} + r_{bias} + w_{r,m} \quad (22)$$

where:

s_r = yaw rate gyro sensitivity

$w_{r,m}$ = yaw rate measurement (gyro) noise

Taking Eq. (22) into account, the system model becomes:

$$\frac{d}{dt} \begin{bmatrix} \psi \\ 1/s_r \\ r_{bias}/s_r \end{bmatrix} = \begin{bmatrix} 0 & r_m & -1 \\ 0 & 0 & 0 \\ 0 & 0 & 0 \end{bmatrix} \begin{bmatrix} \psi \\ 1/s_r \\ r_{bias}/s_r \end{bmatrix} + \begin{bmatrix} w_{r,m} \\ w_{sr} \\ w_{r,bias} \end{bmatrix} \quad (23)$$

where:

$w_{sr}, w_{r,bias}$ = process noises

The yaw Kalman filter can then be constructed using Eq. (22) in place of Eq. (8). With this structure, the sensitivity and bias of the yaw rate gyro are estimated together; the results are shown in Fig. 12. The estimated bias with the sensitivity estimation shows much less variation and appears to have acceptable performance for use in chassis control systems. Although the sensitivity is only observable when the vehicle is maneuvering, its value changes very slowly in the sensors used in this work. Thus some heuristics can be used to estimate the sensitivity on the first few turns a vehicle makes (and perhaps occasionally update this value over the course of a trip) before returning to the original filter structure.

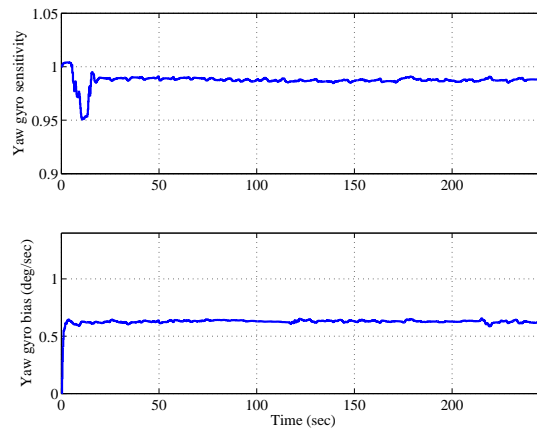


Figure 12 Estimated Yaw Gyro Sensitivity and Bias

7.2 Removing Cross-Coupling in Accelerometers

Since the yaw angle and yaw rate are coupled with the longitudinal and lateral velocities, the accelerometer biases are altered when the filter calibrates the correct yaw gyro sensitivity. The estimated longitudinal and lateral accelerometer biases with the new yaw filter are shown in Fig. 13.

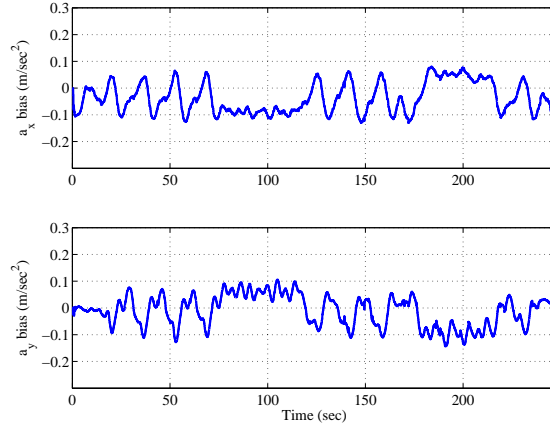


Figure 13 Estimated Accelerometer Biases with New Yaw Angle Estimation

Comparing with the previous results in Fig. 10, little improvement can be seen in these biases. In fact, the a_y bias looks even worse. However, these bias variations can also be explained by correlation with other signals. Figure 14 compares the longitudinal biases with the measured lateral acceleration, showing the similarity between the two signals.

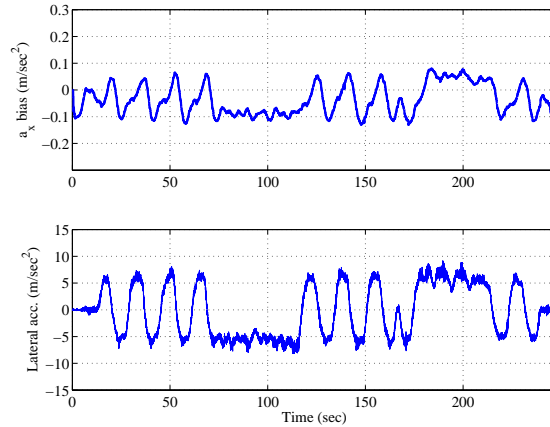


Figure 14 Longitudinal Accelerometer Bias and Lateral Acceleration

Since the longitudinal accelerometer is not exactly aligned with the vehicle's longitudinal axis, the longitudinal accelerometer picks up not only longitudinal acceleration but also lateral acceleration. Therefore, a cross-coupled lateral acceleration component shows up as in the longitudinal accelerometer bias. This component can be explicitly specified and compensated in the previous kinematic relationship for the longitudinal accelerometer.

$$a_{x,m} = \dot{u}_{x,sensor} - \dot{\psi} \cdot u_{y,sensor} + a_{x,bias} + g \cdot \sin \theta_r + c_{x,y} \cdot a_{y,eff} + w_{ax,m} \quad (24)$$

where:

$c_{x,y}$ = cross coupling coefficient from a_y to a_x
 $a_{y,eff} = \dot{u}_{y,sensor} + \dot{\psi} \cdot u_{x,sensor} + g \cdot \sin \phi_t$
 = effective acceleration along lateral axis
 $w_{ax,m} = a_x$ measurement (accelerometer) noise

Fig. 15 shows the comparison between lateral accelerometer bias and lateral acceleration.

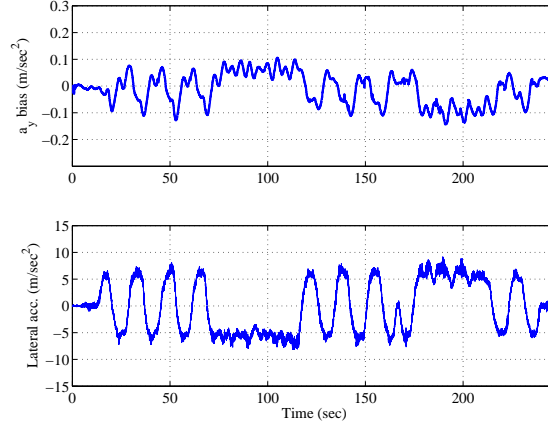


Figure 15 Lateral Accelerometer Bias and Lateral Acceleration

As in the case of the gyro, the lateral accelerometer bias variation has a dependency on the lateral acceleration, which implies there is an error in the sensitivity of the lateral accelerometer. As with the gyro sensitivity estimation, a new sensor kinematic relationship that includes both sensitivity and bias can be defined:

$$a_{y,m} = s_{ay} \cdot (\dot{u}_{y,sensor} + \dot{\psi} \cdot u_{x,sensor} + g \cdot \sin \phi_t) + a_{y,bias} + w_{ay,m} \quad (25)$$

where:

s_{ay} = lateral accelerometer sensitivity

$w_{ay,m} = a_y$ measurement (accelerometer) noise

In order to estimate the cross-coupling coefficient, $c_{x,y}$, Eq. (24) can be integrated and rearranged by defining a term, $\Delta u_x(t)$.

$$\begin{aligned} \Delta u_x(t) &= u_{x,acc}(t) - u_{x,sensor}(t) + \int_0^t (\dot{\psi} \cdot u_{y,sensor} - g \cdot \sin \theta_r) dt' \\ &= a_{x,bias} \cdot t + c_{x,y} \cdot \int_0^t a_{y,eff} dt' + \Delta u_{x,0} + noise \end{aligned} \quad (26)$$

where:

$$u_{x,acc}(t) = \int_0^t a_{x,m} dt'$$

= longitudinal velocity from integrating a_x measurements

Evaluating Eq. (26) at every sample time and rewriting in a linear estimation format gives

$$\begin{bmatrix} \Delta u_x(t_0) \\ \vdots \\ \Delta u_x(t_f) \end{bmatrix} = \begin{bmatrix} t_0 & \int_{t_0}^{t_0} a_{y,eff} dt' \\ \vdots & \vdots \\ t_f & \int_{t_0}^{t_f} a_{y,eff} dt' \end{bmatrix} \begin{bmatrix} a_{x,bias} \\ c_{x,y} \\ \Delta u_{x,0} \end{bmatrix} + noise \quad (27)$$

which is equivalently,

$$z_x = H\hat{x}_x + noise \quad (28)$$

where:

$$\therefore z_x = \begin{bmatrix} \Delta u_x(t_0) \\ \vdots \\ \Delta u_x(t_f) \end{bmatrix}, H = \begin{bmatrix} t_0 & \int_{t_0}^{t_0} a_{y,eff} dt' & 1 \\ \vdots & \vdots & \vdots \\ t_f & \int_{t_0}^{t_f} a_{y,eff} dt' & 1 \end{bmatrix}, \hat{x}_x = \begin{bmatrix} a_{x,bias} \\ c_{x,y} \\ \Delta u_{x,0} \end{bmatrix}$$

Assuming that noise is zero-mean and uncorrelated, a least squares estimator can then be applied to estimate the a_x bias, cross-coupling coefficient, and initial velocity.

$$\hat{x}_x = (H^T H)^{-1} H^T z_x \quad (29)$$

In practice, these assumptions will not strictly hold. However, this simple approach works very well in obtaining reasonable estimates. The estimation is presented as a batch process here since the cross-coupling is essentially static and continuous updating is not required.

Similarly, Eq. (25) can be integrated and rearranged to estimate the lateral accelerometer sensitivity, s_{ay} by defining a term, $\Delta u_x(t)$.

$$\begin{aligned} \Delta u_y(t) &= u_{y,acc}(t) \\ &= a_{y,bias} \cdot t + s_{ay} \cdot (u_{y,sensor}(t) + \int_0^t (\dot{\psi} \cdot u_{x,sensor} + g \cdot \sin \phi_t) dt') + \Delta u_{y,0} + noise \\ &= a_{y,bias} \cdot t + s_{ay} \cdot \int_0^t a_{y,eff} dt' + \Delta u_{y,0} + noise \end{aligned} \quad (30)$$

where:

$$\begin{aligned} u_{y,acc}(t) &= \int_0^t a_{y,m} dt' \\ &= \text{lateral velocity from integrating } a_y \text{ measurements} \end{aligned}$$

Evaluating Eq. (30) at every sample time:

$$\begin{bmatrix} \Delta u_y(t_0) \\ \vdots \\ \Delta u_y(t_f) \end{bmatrix} = \begin{bmatrix} t_0 & \int_{t_0}^{t_0} a_{y,eff} dt' & 1 \\ \vdots & \vdots & \vdots \\ t_f & \int_{t_0}^{t_f} a_{y,eff} dt' & 1 \end{bmatrix} \begin{bmatrix} a_{y,bias} \\ s_{ay} \\ \Delta u_{y,0} \end{bmatrix} + noise \quad (31)$$

which is equivalently,

$$z_y = H\hat{x}_y + noise \quad (32)$$

where:

$$z_y = \begin{bmatrix} \Delta u_y(t_0) \\ \vdots \\ \Delta u_y(t_f) \end{bmatrix}, H = \begin{bmatrix} t_0 & \int_{t_0}^{t_0} a_{y,eff} dt' & 1 \\ \vdots & \vdots & \vdots \\ t_f & \int_{t_0}^{t_f} a_{y,eff} dt' & 1 \end{bmatrix}, \hat{x}_y = \begin{bmatrix} a_{y,bias} \\ s_{ay} \\ \Delta u_{y,0} \end{bmatrix}$$

As before, a least square estimator is applied to estimate the a_y bias, sensitivity, and initial velocity:

$$\hat{x}_y = (H^T H)^{-1} H^T z_y \quad (33)$$

While the sensitivity may change with time, this variation was not found to be particularly large so continuous updating is unnecessary. The estimated cross-coupling coefficient, $c_{x,y}$, and lateral accelerometer sensitivity, s_{ay} , are shown in the Fig. 16.

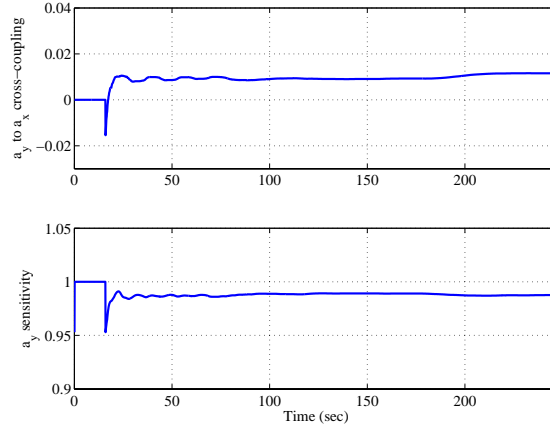


Figure 16 Estimated Cross-coupling Coefficient and Lateral Accelerometer Sensitivity

Taking into account compensation for roll, grade, the cross-coupling coefficient, $c_{x,y}$, and lateral accelerometer sensitivity, s_{ay} , the model for the velocity Kalman filter in Eq. (14) is replaced by the following linear dynamic system constructed from Eq. (24) and Eq. (25):

$$\begin{bmatrix} \dot{u}_{x,sensor} \\ \dot{a}_{x,bias} \\ \dot{u}_{y,sensor} \\ \dot{a}_{y,bias} \end{bmatrix} = \begin{bmatrix} 0 & -1 & r & c_{x,y}/s_{ay} \\ 0 & 0 & 0 & 0 \\ -r & 0 & 0 & -1/s_{ay} \\ 0 & 0 & 0 & 0 \end{bmatrix} \begin{bmatrix} u_{x,sensor} \\ a_{x,bias} \\ u_{y,sensor} \\ a_{y,bias} \end{bmatrix} + \begin{bmatrix} 1 & c_{x,y}/s_{ay} & g & 0 \\ 0 & 0 & 0 & 0 \\ 0 & 1/s_{ay} & 0 & g \\ 0 & 0 & 0 & 0 \end{bmatrix} \begin{bmatrix} a_{x,m} \\ a_{y,m} \\ \sin \theta_r \\ \sin \phi_t \end{bmatrix} + \begin{bmatrix} w_{ax,m} \\ w_{ax,bias} \\ w_{ay,m} \\ w_{ay,bias} \end{bmatrix} \quad (34)$$

where:

$$w_{ax,bias}, w_{ay,bias} = \text{process noises}$$

Figure 17 shows the estimated accelerometer biases after the cross-coupling between the two accelerometers and lateral accelerometer sensitivity are taken into account.

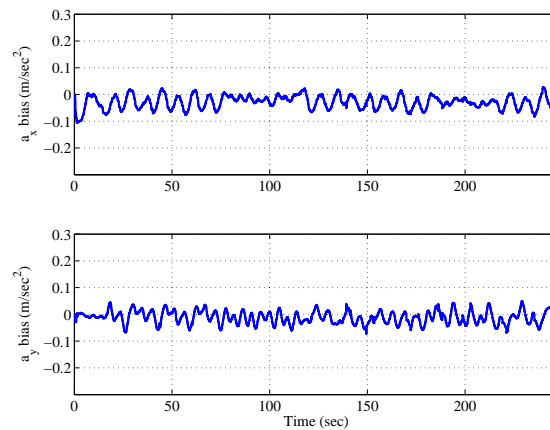


Figure 17 Estimated Accelerometer Biases after the Compensation

Note that the variations are reduced after the compensation. Since the lateral acceleration tends to dominate over longitudinal acceleration, only cross-coupling from the lateral acceleration to the longitudinal accelerometer and the lateral accelerometer

sensitivity are considered. Estimation of other sensitivity or cross-coupling parameters could be included in an analogous manner but, since the signals are somewhat lower, more convergence time is necessary and the resulting improvement is less. Obviously, there are some remaining bias variations, but the absolute level of variation is quite small given the relatively simple vehicle model used for estimation purposes.

In fact, a large portion of the remaining bias in longitudinal acceleration can be traced to a single modeling assumption. Rapid grade fluctuations at certain spatial frequencies are not detectable through the velocity based grade estimate. As the vehicle moves along the road, the rear wheels see almost the same input as the front wheels, delayed in time by the interval equal to the wheelbase divided by speed. This time delay acts to filter the bounce and pitch motion of the vehicle, and has been called wheelbase filtering [21]. The typical effects of wheelbase filtering are illustrated in Fig. 18.

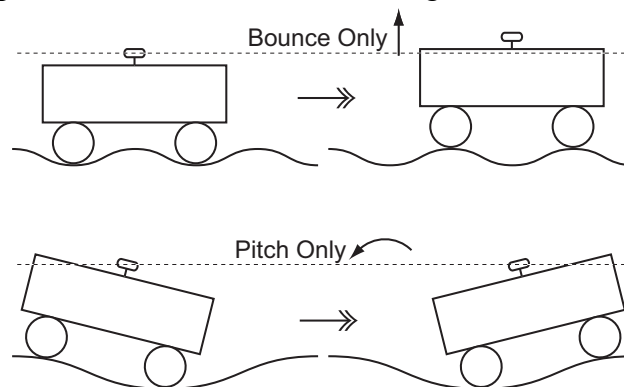


Figure 18 Wheelbase Filtering Mechanism

When the wavelength of the road is equal to the wheelbase of the vehicle, or integer multiples equal to the wheelbase, the vehicle only bounces up and down without a pitch change. Similarly, only pitch motion occurs when the wavelength is equal to twice the wheelbase or odd integer multiples equal to twice the wheelbase length. In either case, at these frequencies, the velocity based grade estimate does not reflect the true grade seen by the vehicle. While this effect is small for most roads, the parking lot structure used for testing has a pronounced periodic texture (comparable to the lower half of Fig. 18) to provide for drainage. Thus the unmodeled dynamics reflected in the bias variation in Fig. 17 have an easily understood physical interpretation in light of the assumptions made in grade measurement. The fact that such seemingly small effects appear provides some additional measure of confidence that the estimator is correctly capturing the larger vehicle motion.

8. STATISTICAL ANALYSIS OF THE KALMAN FILTERS

In the previous sections, the vehicle state estimates are compared to predictions from a calibrated model instead of actual truth. This is a result of the difficulty involved with obtaining truth measurements for speed over ground. Optical systems do exist but are far more expensive than the even the research version of the system presented here and suffer from some inaccuracies of their own. It is possible, however, to offer additional

support for the filter performance by comparing the innovation statistics to the predictions obtained by propagating the sensor and process noise covariances through the Kalman filters. As this section shows, simple prediction from a linear Kalman filter analysis describes the experimental behavior quite accurately.

The unique structure of the Kalman filters used in this paper make it possible to develop a statistical analysis easily given only the specifications of the INS sensors and GPS receivers. This follows from the fact that all the system models for the Kalman filters are purely based on the kinematic relationships between the INS sensor measurements and the vehicle states as shown in Eq. (22) and Eq. (34). This means that the system model noises (process noises) are mainly from the INS sensor noises, assuming that the biases and sensitivities of the INS sensors can be modeled as random walks with relatively small variances. As a result, noises from the INS sensors, such as accelerometers and rate gyros, act as the process noises in the Kalman filters and the noise from the GPS system enters as traditional measurement noise in Eq (7) and Eq. (19).

Table 1 shows the actual values for the process noise variances of the Kalman filters used in this paper. The noise variances of the accelerometers and the rate gyros are taken from the sensor specification and are used as the process noise variances for the corresponding vehicle states. The noise variances for the sensor sensitivities and biases are chosen from the experimental tests to give reasonable convergence rates of the sensitivity and bias estimates. The numerical values for the measurement noise variances of the Kalman filters are also shown in Table 1. The noise covariances of the GPS angle and velocity measurements are taken from the GPS receiver specifications and are used as the measurement noise variances for each Kalman filter.

Process Noise				Measurement Noise	
State	1σ	State	1σ	Measurement	1σ
$w_{r,m}$	0.2 (deg/s)	$w_{ax,m}$	0.05 (m/s ²)	ψ_m^{GPS}	0.2 (deg)
w_{sr}	1.0e-3	$w_{ay,m}$	0.05 (m/s ²)	$u_{x,m}^{GPS}$	0.03 (m/s)
$w_{r,bias}$	1.0e-2 (deg/s)	$w_{ax,bias}, w_{ay,bias}$	1.0e-3 (m/s ²)	$u_{y,m}^{GPS}$	0.03 (m/s)

Table 1 Measurement and Process Noise Covariances

With these noise variances, the estimate error covariances can be calculated from the Kalman filters under the assumption that all calibration is correct and all compensation is performed exactly. These covariances describe the differences between the filter output and ground truth, however, and are not directly comparable to the measurement residual (or innovation) obtained by comparing the filter output to the measurement at each time step. For a proper comparison, the expected variances of the measurement residuals may be calculated as the sum of the error covariances from the Kalman filters and the variances of the measurement noises as shown in Eq. (35), assuming that the process and measurement noises are uncorrelated.

$$S = CPC^T + R \quad (35)$$

where:

S = measurement residual covariance

C = observation matrix

P = error covariance matrix

R = measurement noise covariance

Yaw Filter	Measurement Residuals				Expected Variances	
	Mean	-4.1e-3	1σ	0.2572	1σ	0.2544
Velocity Filter	Measurement Residuals				Expected Variances	
	Mean	-1.3e-4	1σ	0.04037	1σ	0.03852
Percentages within σ Bounds						
Yaw Filter	$< 1\sigma$	71.57%	$< 2\sigma$	94.90%	$< 3\sigma$	98.83%
Velocity Filter	$< 1\sigma$	69.88%	$< 2\sigma$	95.54%	$< 3\sigma$	99.08%
Gaussian (Normal)	$< 1\sigma$	68.27%	$< 2\sigma$	95.45%	$< 3\sigma$	99.73%

Table 2 Statistics of Measurement Residuals and Estimated Variances

The statistics of the actual measurement residuals from the experimental tests are shown in Table 2 together with the expected variances of the measurement residuals. It can be clearly seen that the variances of measurement residuals are similar to the Kalman filter predictions. This suggests that the calibration and compensation methods function as desired. In reality, the sensor performance is slightly better than that guaranteed by the manufacturer but in these experiments this conservatism neatly balances degradation due to unmodeled effects such as wheelbase filtering. Table 2 also demonstrates that the mean values of the measurement residuals are virtually zero. This implies that the techniques for the sensor bias removal work and no serious biases exist during the estimation processes. The distributions of the measurement residuals are also compared with the Gaussian (normal) distribution in the last three columns of Table 2. The comparison shows that the measurement residuals follow the normal distribution roughly. This indicates that the basic assumption of this analysis (zero-mean Gaussian noise) is reasonable and that the Kalman filter error prediction is in fact meaningful. Figure 19 shows the plot of measurement residuals for each Kalman filter and the bounding 3σ regions of confidence derived from the filter. Note that measurement residuals are centered at zero and most of them are within the bounding 3σ regions. The outliers, in fact, correspond to points where new GPS data was not available for a given time step, an effect that could be explicitly included in calculating the expected variances but was not considered here.

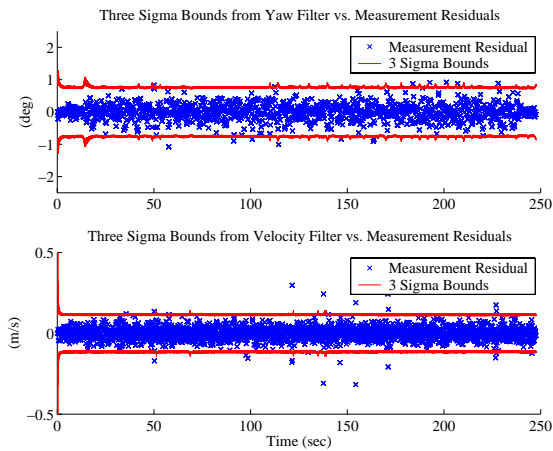


Figure 19 Measurement Residual vs. Estimated 3σ Bounds

9. CONCLUSIONS

With the combination of a two-antenna GPS receiver and four automotive grade inertial sensors (two rate gyros and two accelerometers), it is possible to develop an estimate of vehicle sideslip corrected for roll and grade effects. The proposed method provides high update estimates of sideslip, longitudinal velocity, roll and grade and compares well to predictions from calibrated models and Kalman filter analysis. The complete system calibrates the inertial sensor sensitivities and biases at appropriate update rates and can handle loss of the GPS signal for periods of time by simply integrating the calibrated inertial sensors. The vehicle states obtained by this system represent a new level of fidelity for vehicle control and have been successfully implemented in steer-by-wire control [4] and for tire cornering stiffness estimation. Future work will use this feedback system for rollover avoidance intervention, operation of by-wire systems at the limits of handling and highly detailed steering force feedback for the driver.

10. ACKNOWLEDGEMENTS

The authors would like to thank the Robert Bosch Corporation for sponsoring this work and providing the test vehicle and sensors. Special thanks to Dr. Jasim Ahmed of the Bosch RTC in Palo Alto, CA, for helpful input and discussion. The authors also would like to thank the reviewers for motivating the statistical analysis of the Kalman filters.

REFERENCE

- [1] Nishio, A., et. al., 2001, "Development of Vehicle Stability Control System Based on Vehicle Sideslip Angle Estimation," SAE Paper No. 2001-01-0137.
- [2] Kimbrough, S., 1991, "Coordinated Braking and Steering Control for Emergency Stops and Accelerations," *Proc. of ASME WAM*, Atlanta, GA, pp. 229-244.
- [3] Fukada, Y., 1999, "Slip-Angle Estimation for Vehicle Stability Control," *Vehicle System Dynamics*, **32**(4), pp. 375-388.

- [4] Yih, P., Ryu, J., Gerdes, J. C., 2003, "Modification of Vehicle Handling Characteristics via Steer-by-wire", *Proc. of American Control Conf.*, Denver, CO, pp. 2578-2583.
- [5] Farrelly, J., and Wellstead, P., 1996, "Estimation of Vehicle Lateral Velocity," *Proc. of IEEE Conf. on Control Applications*, pp.552-557.
- [6] Ungoren, A. Y., Peng, H., Tseng, H. E., 2002, "Experimental Verification of Lateral Speed Estimation Methods", *Proc. of AVEC 2002- Int. Symp. on Advanced Vehicle Control*, Hiroshima, Japan, pp. 361-366.
- [7] Berman, Z., Powell, J. D., 1998, "The Role of Dead Reckoning and Inertial Sensors in Future General Aviation Navigation," *Proc. of IEEE Position Location and Navigation Symp.*, pp. 510-517.
- [8] Da, R., Dedes, G., Shubert, K., 1996, "Design and Analysis of a High-Accuracy Airborne GPS/INS System," *Proc. of Int. Technical Meeting of the Satellite Division of the Institute of Navigation (ION GPS-96)*, pp. 955-964.
- [9] Gebre-Egziabher, D., Hayward, R. C., Powell, J.D., 1998, "A Low-Cost GPS/Inertial Attitude Heading Reference System (AHRS) for General Aviation Application," *Proc. of IEEE Position Location and Navigation Symp.*, pp. 518-525.
- [10] Gebre-Egziabher, D., Powell, J. D., Enge, P., 2001, "Design and Performance Analysis of a Low-Cost Aided Dead Reckoning Navigation System," *Gyroscopy and Navigation*, 4(35), pp. 83-92.
- [11] Bevely, D. M., et. al., 2000, "The Use of GPS Based Velocity Measurements for Improved Vehicle State Estimation.", *Proc. of American Control Conf.*, Chicago, IL, pp. 2538-2542.
- [12] Masson, A., Burtin, D., Sebe, M., 1996, "Kinematic DGPS and INS Hybridization for Precise Trajectory Determination," *Proc. of Int. Technical Meeting of the Satellite Division of the Institute of Navigation (ION GPS-96)*, pp. 965-973.
- [13] Bevely, D. M., Sheridan, R., and Gerdes, J. C., 2001, "Integrating INS Sensors with GPS Velocity Measurements for Continuous Estimation of Vehicle Sideslip and Tire Cornering Stiffness", *Proc. of American Control Conf.*, Arlington, VA, pp. 25-30.
- [14] Tseng, H. E., 2000, "Dynamic Estimation of Road Bank Angle", *Vehicle System Dynamics*, 4(4-5), pp. 307-328.
- [15] Bae, H. S., Ryu, J., and Gerdes, J. C., 2001, "Road Grade and Vehicle Parameter Estimation for Longitudinal Control Using GPS," *Proc. of IEEE Conf. on Intelligent Transportation Systems*, Oakland, California, pp. 166-171.
- [16] IntegriNautics, AutoFarm GPS Precision Farming, <http://www.integrinautics.com/AutoFarm/systems.html>.
- [17] Dixon, J. C., 1996, *Tires, Suspension and Handling*, Society of Automotive Engineers, Inc., Warrendale, PA.
- [18] Milliken, W. F., Milliken, D. L., 1995, *Race Car Vehicle Dynamics*, Society of Automotive Engineers, Inc., Warrendale, PA.
- [19] Ryu, J., Rossetter, E. J., Gerdes, J. C., 2002, *Proc. of AVEC 2002 - Int. Symp. on Advanced Vehicle Control*, Hiroshima, Japan, pp. 373-380.
- [20] Chen, B., and Peng, H., 1999, "Rollover Warning of Articulated Vehicles Based on a Time-to-Rollover Metric", *ASME Dynamic Systems and Control Division (Publication) DSC-Vol.67 IMECE*, pp. 247-254.

- [21] Gillespie, T. D., 1992, *Fundamentals of Vehicle Dynamics*, Society of Automotive Engineers, Inc., Warrendale, PA.
- [22] Gelb, A., et. al., 1974, *Applied Optimal Estimation*, The M.I.T. Press, Cambridge, MA.
- [23] Stengel, R. F., 1994, *Optimal Control and Estimation*, Dover Publications, Inc., Mineola, NY.

List of Figures

- Figure 1 Bicycle Model
- Figure 2 Yaw Angle Estimates
- Figure 3 Yaw Rate and Sideslip Angle Estimates
- Figure 4 Longitudinal Accelerometer Bias and Grade Estimates
- Figure 5 Lateral Accelerometer Bias and Roll Angle
- Figure 6 Roll Center Model with Grade and Bank Angle
- Figure 7 Comparison of Sideslip Angle Estimates
- Figure 8 Longitudinal Velocity Estimates
- Figure 9 Roll Angle Estimates
- Figure 10 Estimated Accelerometer Biases
- Figure 11 Estimated Yaw Gyro Bias and Yaw Rate
- Figure 12 Estimated Yaw Gyro Sensitivity and Bias
- Figure 13 Estimated Accelerometer Biases with New Yaw Angle Estimation
- Figure 14 Longitudinal Accelerometer Bias and Lateral Acceleration
- Figure 15 Lateral Accelerometer Bias and Lateral Acceleration
- Figure 16 Estimated Cross-coupling Coefficient and Lateral Accelerometer Sensitivity
- Figure 17 Estimated Accelerometer Biases after the Compensation
- Figure 18 Wheelbase Filtering Mechanism
- Figure 19 Measurement Residual vs. Estimated 3σ Bounds

List of Tables

- Table 1 Measurement and Process Noise Covariances
- Table 2 Statistics of Measurement Residuals and Estimated Variances